LAWRENCE
LIVERMORE
NATIONAL
LABORATORY

LLNL-TR-406039

# Development of Standards for NanoSIMS Analyses of Biological Materials

M.L. Davission, P.K. Weber, J. Pett-Ridge, S. Singer

August 5, 2008

## Disclaimer



This work performed under the auspices of the U.S. Department of Energy by Lawrence Livermore National Laboratory under Contract DE-AC52-07NA27344.

DHS National Laboratory R&D Program Report:

# Development of Standards for NanoSIMS Analyses of Biological Materials

M. Lee Davisson, Peter K. Weber, Jennifer Pett-Ridge, Steven Singer

Lawrence Livermore National Laboratory

Thrust Area: Forensics and Attribution, Chemical and Physical Analysis

Date Submitted**:** July 31, 2008

**Performer Points of Contact:**

| Focus Area Lead | **Organization** | Phone | Email |
|---|---|---|---|
| Stephan P. Velsko | LLNL | 925-423-0191 | Velsko2@llnl.gov |
| **Principal Investigators** | **Organization** | **Phone** | **Email** |
| Peter K. Weber | LLNL | 925-422-3018 | Weber1@llnl.gov |

**Table of Contents**

## Executive Summary

NanoSIMS is a powerful analytical technique for investigating element distributions at the nanometer scale, but quantifying elemental abundances requires appropriate standards, which are not readily available for biological materials. Standards for trace element analyses have been extensively developed for secondary ion mass spectrometry (SIMS) in the semiconductor industry and in the geological sciences. The three primary approaches for generating standards for SIMS are: (1) ion implantation (2) using previously characterized natural materials, and (3) preparing synthetic substances. Ion implantation is a reliable method for generating trace element standards, but it is expensive, which limits investigation of the analytical issues discussed above. It also requires low background levels of the elements of interest. Finding or making standard materials has the potential to provide more flexibility than ion implantation, but realizing homogeneity at the nano-scale is in itself a significant challenge.

In this study, we experiment with all three approaches, but with an emphasis toward synthetic organic polymers in order to reduce costs, increase flexibility, and achieve a wide dynamic concentration range. This emphasis serves to meet the major challenge for biological samples of identifying matrix matched, homogeneous material. Biological samples themselves are typically heterogeneous at the scale of microns to 100s of microns, and therefore they are poor SIMS standards. Therefore, we focused on identifying “biological-like” materials—either natural or synthetic—that can be used for standards. The primary criterion is that the material be as compositionally similar to biological samples as possible (primarily C, H, O, and N).

For natural material we adsorbed organic colloids consisting of peptidoglycan (i.e., amino sugars), activated charcoal, and humic acids. Experiments conducted with Si on peptidoglycan showed low affinity as $SiO_2$, yet its distribution in the matrix was similar to that observed in spores. In experiments with Mo on humic acid, homogeneity was achieved and a sensitivity factor relative to C was determined.

For synthetic material, we successfully prepared polyacrylic acid containing complexed elements of Mo, Ca, Sr, and Ba at low abundance. These were prepared as aqueous mixtures of dissolved elements and polyacrylic resin, followed by thin film drying. The Mo was homogeneously distributed and yielded a relative sensitivity factor nearly identical to that calculated for humic acid. This approach shows great promise for most water soluble metals.

Poly(methacrylate) thin films were prepared that contained different low-level concentrations of Si introduced as a silane compound. Although homogeneity was not fully achieved, the analytical results did validate our previous quantitative methodology for Si. In addition, Commercial plastics were also examined for

suitability for F and Cl. We found food-grade polyvinyl tubing produced high precision Cl determinations.

For ion implantation, we used epoxy as the substrate and successfully extracted depth profiles and sensitivity factors for F and Cu.

## INTRODUCTION

The small scale (nanometer) offered by NanoSIMS analyses provides a unique measurement opportunity to study elemental processes at high spatial resolution in a variety of complex samples (Bradley, et al. 2005; Badro, et al. 2007; Moreau, et al. 2007; Popa, et al. 2007; Ghosal, et al. 2008. However, this approach encounters challenges for standardization similar to that experienced in other SIMS techniques (Wilson et al., 1989). This relates mostly to needing a standard of known concentration in a similar material as the sample of interest. The most important characteristic of an appropriate standard is that it has the major element composition of the material of interest ("matrix matched"). Standardization is achieved by normalizing the yield of the elements of interest to a major element of known abundance within the matrix. Normalization relies on the relative yield of the elements of interest and major element be known for the sample. This relative yield can change by a factor of 2 to 3 based on matrix composition. This is because ionization efficiency is both element and material dependent (Wilson et al., 1989). For example, the ionization efficiencies of carbon and chlorine implanted into the same Si-wafer differ nearly 7-fold. Additionally, elements of low concentration (e.g., ppm) in a matrix typically ionize more efficiently than if it were at high concentration (percent levels).

Standards also provide a method to determine the importance of molecular species that co-occur at the nominal mass of interest (isobaric interferences). At lower masses, interfering species can typically be resolved with the NanoSIMS high mass resolving power (e.g., the mass difference of 0.044 atomic mass units between $^{44}Ca$ and $^{28}Si^{16}O$ can readily be resolved), but at higher masses, this can become more difficult, depending on the interference. Standards that match the major and minor element composition of the unknown allow for the evaluation of the importance of interferences. Finally, standards allow for analytical characteristics to be determined, including detection limit, reproducibility, accuracy and precision, and they provide a control for variation in instrument tuning.

Biological materials consist mostly of carbon, hydrogen, oxygen, and nitrogen with minor levels of phosphorus and sulfur. These together form molecular structures dominated by lipids, sugars, and proteins. The approach taken in this study is to investigate the use of various organic polymers and also organic extracts of natural material as potential matrices for biological standards. For expedience, in most cases we used readily available material to test our methods for introducing known quantities of an element of interest. The challenge was to

fix these elements homogeneously at the nanometer scale in order to facilitate repeatable measurements and quantitative results.

In previous work in our laboratory, a set of organic Ca standards (1.3, 3.3, 3.4, 7.3, 14.5, 28.9 µg/g) were generated at the University of Missouri at Columbia in the lab of Prof. David Robertson. Their approach was to use standard epoxy resin as the organic matrix. Ca was uniformly dispersed in the epoxy by complexing it with crown ether. The standards generated a reasonable working curve, but the dynamic range of concentration was very small. In this work, we sought to extend the dynamic range and simplicity of with which standards could be fabricated.

A range of elements were investigated that span both metals and non-metals and include Ca, Sr, Ba, Mo, Cu, Si, F, and Cl. It is not possible to identify a "biological-like" material compatible with all these elements. Consequently, for metals (transition elements and alkaline earths) emphasis was placed on coordination into a natural and synthetic material such as humic acid and polyacrylic acid, which both have high density of carboxylic acid function. This approach proved highly successful for Mo and initial work showed potential for alkaline earth elements prepared as soluble acetates. In the case of Cu, an ion-implant in epoxy was available and was used for a measurement instead. For a challenging non-metal like Si, adsorption to amide groups on peptidoglycan was achieved, and separately a hydrophobic interaction between a silane compound and poly(methacrylate) was moderately successful. For F and Cl, both an ion-implant and commercial polymers were successfully measured. Because F and Cl are commonly substituted into organic polymers, this source may be an immediate practical solution for standards.

Below is presented in order details of sample preparation and NanoSIMS results for Si and Mo. This is followed by brief results from Ca, Sr, Ba, Cl, and F. Following these results is a discussion with interpretation of data and derivation of relative sensitivity factors where data is adequate. Note that additional materials were initially explored for their potential as a Si standard and their results are discussed in Appendix 1.

## SILICON

### NATURAL ORGANIC COLLOIDS

Natural organic matter residues have the potential to complex elements in a manner that is comparable to the biomolecules in spores. These residues are abundant in the environment and can be found in water, soil, and air. They are residues formed as abiotic byproducts of biological production and decay, or by condensation/adsorption reaction in the case of atmospheric aerosols. Their size widely varies, but from the standpoint of this investigation we are most interested in isolating fractions of natural organic matter that we arbitrarily designate as colloidal size, which we operationally define as isolated material with a size range between 3500 Daltons and 1.0 um. In addition, colloidal material that would be of

most interest is the size fraction that has molecular character similar to bacterial spore coating material.

Most bacteria are surrounded by a cell wall comprised of glycoprotein material, which has various confirmations of polysaccharides structures with N-acetyl linkages. In vegetative cells this cell wall structure is known collectively as peptidoglycan (Seltmann and Holst, 2002), whereas in spores peptidoglycan predominates in the inner-coat to outer cortex region (Henriques and Moran, 2000). These structures provide a molecular backbone for covalent attachment of proteins and lipids, which in congress with enzymatic activity serves as an important transport and defensive barrier to the external environment. Note that upon sporulation, the peptidoglycan undergoes transformation in molecular ordering, and then is encased in various protein structures known as the inner and outer cortex (Henriques and Moran, 2000).

More relevant to the current discussion, peptidoglycans will lyse when a bacteria dies and will form colloid residue in its immediate environment. These residues have been isolated from terrestrial water sources (Leenheer et al, 2004). One of the main interests in this material is its potential affinity for silica because of its similarity to living bacterial cell walls. Therefore, organic colloids isolated from natural water were used in several silica adsorption experiments. The procedures for isolation of organic colloids are documented elsewhere (Leenheer et al., 2004, 2008), but are briefly outlined in Appendix 2. The isolated extract used for the silica adsorption experiments was archived organic material isolated from street runoff collected during a rain storm at Livermore, CA and processed in August 2003. Although the colloidal fraction of this organic material shows structural evidence similar to peptidoglycan, its dark brown color as a dried isolate suggests that it has been complexed with humic-like material, which is commonly at high concentration in street runoff. In order to maximize the potential of silica adsorption, the colloids were subjected to a deacylation step by boiling 50 mg of isolate dissolved in 100 ml of 6N NaOH at 112°C for 90 minutes. This step should have broken many of the ether and ester linkages in the material and maximized free hydroxyl end-members (Chang et al., 2001). After the deacylation step, this solution was isolated in a 3500 Dalton dialysis bag and dialyzed against distilled water until a minimum electrical conductivity was reached (5 uS). A dark brown precipitate formed in the dialysis bag and the remaining solution was notably lighter in color. This precipitate was separated by centrifugation and the lighter color solution was used directly in the adsorption experiments.

Three separate adsorption experiments were conducted using this colloidal isolate. All three used a measured volume of the dissolved colloid mixed with an equal volume of a 156 mg/L $SiO_2$ solution. This provided a weight ratio of $SiO_2$ to colloid of >1:3. Note that some colloid material was lost during the deacylation step and the final mass of colloid was not measured. Therefore, the exact $SiO_2$ to colloid ratio is not known. The $SiO_2$ solution was prepared by adding a measured

amount of cabosil to distilled water and heating it to near boiling for a few minutes until the solution was clear. Aliquots used for the adsorption experiment were filter at 0.45 μm beforehand. The $SiO_2$ concentration was determined using the molybdate yellow colorimetric method (Standard Methods, 2005). Note that the amount of $SiO_2$ added to the colloid solution was well in excess of any adsorption capacity, so that the $SiO_2$ concentration should not have appreciably changed during the adsorption, although for this experiment it was not measured following adsorption. In addition, although aliquots of the $SiO_2$ solution were filter at 0.45um before addition to the colloid solution, it is likely that the $SiO_2$ occurred both in a monomeric and oligiomeric form. After $SiO_2$ addition, the two solutions were mixed and then dialyzed against distilled water in a 3500 Dalton bag. This was followed by freeze-drying. The first experiment mixed the $SiO_2$ and colloid solution at pH=10.6, adjusted using 3N NaOH. The second experiment mixed the solution at low pH ~2 using concentrated HCl. For the third experiment, a stoichiometric excess of $Ca(NO_3)_2 \cdot 4H_2O$ was added to the mixture to determine potential effects of cation bridging on $SiO_2$ adsorption. Note that for this third experiment, a small amount of the colloid precipitated overnight. This precipitate was removed by centrifugation before dialysis. Freeze-dried material was mounted on a aluminum bullet by simply tapping onto the bullet a small amount electrostatically attached to the tip of a metal scribing instrument. The bullet was then gold-coated.

Figure 1 shows a typical NanoSims image of the natural organic colloid. Note the spheroidal shape of the individual particles at sizes roughly approaching those of spores. The clumping habit is likely due to electrostatic attraction. The colloids are well defined by carbon or nitrogen abundances, which were used to normalize the Si ion counts. However, the aluminum bullets used to mount the samples contributed to an unusually high Si background contamination. This required quantifying regions of interest within the particles in order to differentiate Si associated only with the particles. Nevertheless, overall the high background did affect the quality of the quantitative procedures used to process the data, and follow-up work with peptidoglycans presented below avoided using the aluminum bullets. Regardless of its shortcomings, the Si image does show a readily measurable amount of Si associated with the colloid particles. The distribution of the Si is somewhat heterogeneous and at relatively low abundance.

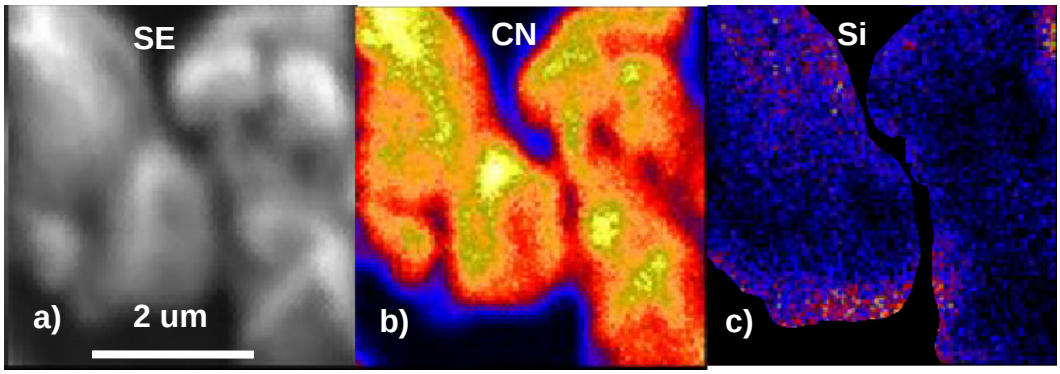

**Figure 1**. NanoSims images of natural organic colloids show spheroidal particles with dimensions similar to spores. Samples were prepared by equilibrating with a 156 mg/L solution of dissolved $SiO_2$. Si distribution in this sample prepared under high pH conditions is somewhat heterogeneous, but forms a low-level abundance clearly associated with the particle.

Comparison is made among the Si/C ratios for these natural organic colloids samples prepared and analyzed using the three different experimental conditions outlined above (see Table 1). For the adsorption conducted at high pH, the Si/C ratio on four separate NanoSims images ranged from 0.007 to 0.024. The first two images showed stable Si/C ratios over the majority of the particle depth, whereas the remaining two images showed dramatic increases with depth. However, these latter two particles had constant ratios in the early part of the analysis that were somewhat lower than those of the former, and these data were used in the final analysis.

**Table 1.** Mean Si/C ratios for organic colloids

| Concentration | $^{28}Si/^{12}C$ ratio | $^{28}Si/^{12}C$ std dev. |
|---|---|---|
| **High pH** | 0.024 | 0.007 |
| | 0.022 | 0.005 |
| | 0.007 | 0.001 |
| | 0.009 | 0.002 |
| | | |
| **Low pH** | 0.0140 | 0.0002 |
| | 0.0074 | 0.0001 |
| | 0.0129 | 0.0001 |
| | | |
| **Ca addition** | 0.0462 | 0.0011 |
| | 0.0517 | 0.0022 |
| | 0.0193 | 0.0016 |

For the sample prepared under low pH conditions, the Si/C ratio observed in three separate particle analyses suggested a slightly lower value, but additional analysis are probably needed to confirm this. However, of the three spots analyzed on colloids prepared with the Ca-modified solution, it was very clear that the Si was more heterogeneously distributed and quantitatively formed higher Si/C ratios. In one image, it was noted that the core of the particle was acting as an insulator and charging under the Cs beam, which contrasted with outer carbon–rich portions (Figure 2). This image suggests that the Ca in solution may have reacted with the silica and formed an oxide mineral around which the colloids adsorbed.

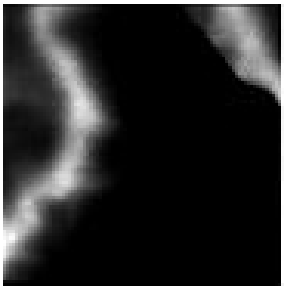

**Figure 2.** SEM image of a natural colloid particle exposed in a Ca-enriched $SiO_2$ solution. The image shows evidence of surface charging in the core, but not in the outer regions.

## PEPTIDOGLYCANS

A peptidoglycan isolate of *Bacillus subtilis* was purchased (Sigma-Aldrich 69554 Fluka Biochemika) for this experiment. The isolate was likely prepared by a standard method using physical agitation (ultrasonication, freeze/thaw, grinding) to lyse the cell wall followed by ultracentrifugation (Seltmann and Holst, 2002). A total of 10 mg was added to 50 ml of distilled water. The poor solubility of the peptidoglycan required addition of 100 uL of 3N NaOH and equilibration overnight in order to disperse uniformly in solution. This solution was placed in a 3500 Dalton dialysis bag and dialyzed against distilled water until a low conductivity was reached. Note that the peptidoglycan remained dispersed. The dialysis bag was then dialyzed overnight against one liter of solution with 47 mg/L dissolved $SiO_2$. The dialysis bag content was then dialyzed against distilled water until a minimum $SiO_2$ concentration was reached, followed by freeze-drying of the bag contents. Freeze-dried material was pressed into gold by using a small amount electrostatically attached to the tip of a metal scribing instrument.

Figure 3 below illustrates a typical NanoSIMS image of a single peptidoglycan particle exposed to the $SiO_2$ solution. Comparison of the C and Si distributions shows the relatively low abundance of Si compare to C, but the fact that Si is distinctly observed and somewhat evenly distributed throughout the particle indicates some affinity between the peptidoglycan and the $SiO_2$ in aqueous media.

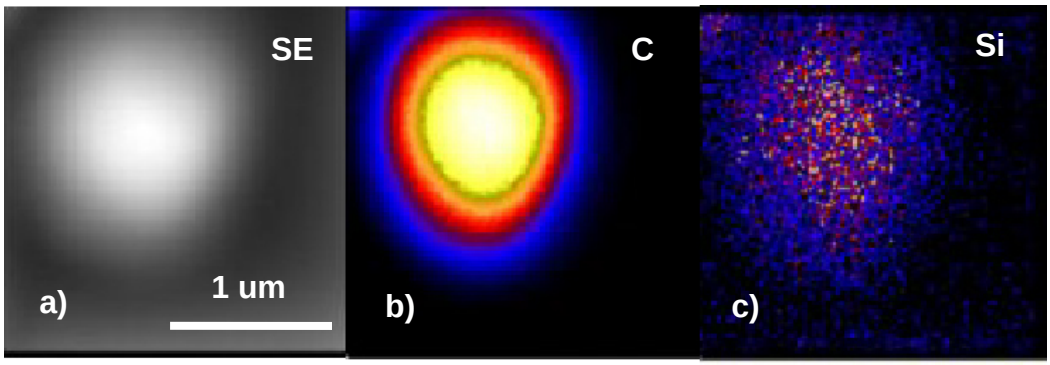

**Figure 3.** Single particle of peptidoglycan prepared by equilibrating with a 47 mg/L $SiO_2$ solution, followed by equilibration with distilled water until a minimum $SiO_2$ concentration was reached. a) Secondary electron (SE) image shows the spherical character of the particles, and b) carbon and c) silicon are evenly distributed.

Analysis of the Si/C ratio over the area of the particle (Figure 4) shows that near the surface the ratio is relatively low, but climbs nearly two orders of magnitude during the course of the analysis. In this particular sample particle, the entire material was sputtered and is represented by the 41 planes of analysis in Figure 4. Surprisingly, the SI/C ratio does not peak until very near the end of the analysis.

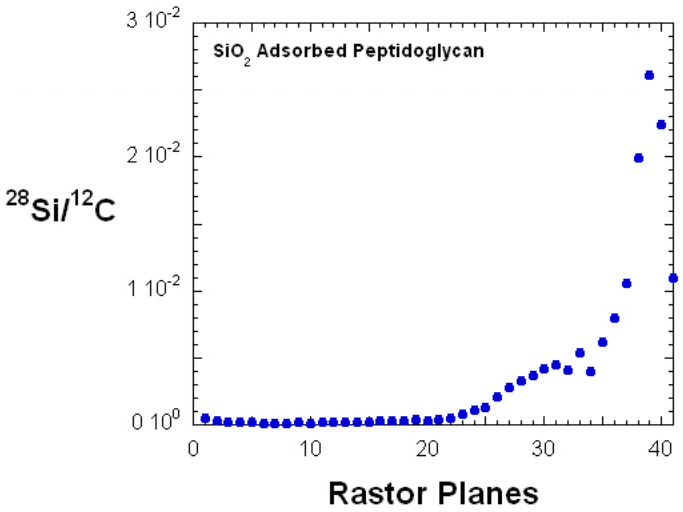


**Figure 4.** The Si/C ratio of the particle imaged in Figure 3 shows a progression from low to high values during the course of sputtering through the entire sample.

Further analysis shown in Figure 5 indicates all particles analyzed on this sample exhibited the same behavior in Si/C ratio during the course of the analysis. Whereas in a uniform distribution of Si in the carbon matrix the Si/C ratio should show little variation with depth, the particles here suggest either an uneven distribution related somehow to the compositional structure or to a migration of the Si downward during the course of analysis. Nevertheless, a simple arithmetic mean of the Si/C ratios for each spot analyzed yield a mean Si/C ratio of $4.3 \times 10^{-3}$ $\pm 0.8 \times 10^{-3}$ (Table 2). Assuming that the peptidoglycan comprises 50% carbon by weight, this suggests a Si concentration of ~2000 ppm.

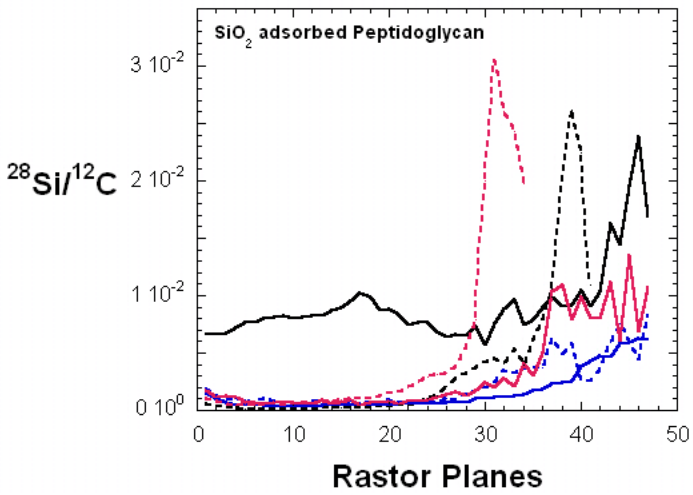


**Figure 5**. Si/C ratios of all particles measured for the $SiO_2$ adsorbed peptidoglycan sample indicate a progressive rise in ratio with sputtering depth in the particle. Rastor size in the data ranges from 2 to 10 um.

**Table 2**. Mean Si/C ratios of Bacillus *subtilis* peptidoglycan extract

| Concentration | $^{28}Si/^{12}C$ ratio | $^{28}Si/^{12}C$ std dev. |
|---|---|---|
| **$SiO_2$ adsorbed** | 0.0093 | 0.0011 |
| | 0.0036 | 0.0007 |
| | 0.0019 | 0.0001 |
| | 0.0025 | 0.0006 |
| | 0.0037 | 0.0001 |
| | 0.0050 | 0.0007 |
| | | |
| **HF treated** | 0.00012 | 0.00001 |
| | 0.00018 | 0.00012 |
| | 0.00110 | 0.00011 |
| | 0.00088 | 0.00099 |

For comparison purposes, another 10mg of *Bacillus subtilis* peptidoglycan was placed into a 3500 Dalton dialysis bag and dialyzed overnight against 0.1N HF, followed by dialysis against distilled water until a minimum conductivity was reached. The bag contents were then freeze-dried. This sample of peptidoglycan was prepared in order to remove $SiO_2$ potentially present on the material as received from the vendor. The analysis provides minimum Si detected on this material for comparison to adsorption experiments.

Figure 6 below shows NanoSIMS images of HF-treated peptidoglycan. The large raster size incorporates several individual particles, although they appear to have a more platy habit compared to the $SiO_2$ adsorbed material. However, there is a notable absence of Si counts in the image compared to the carbon, suggesting a much diminished concentration due to the HF extraction.

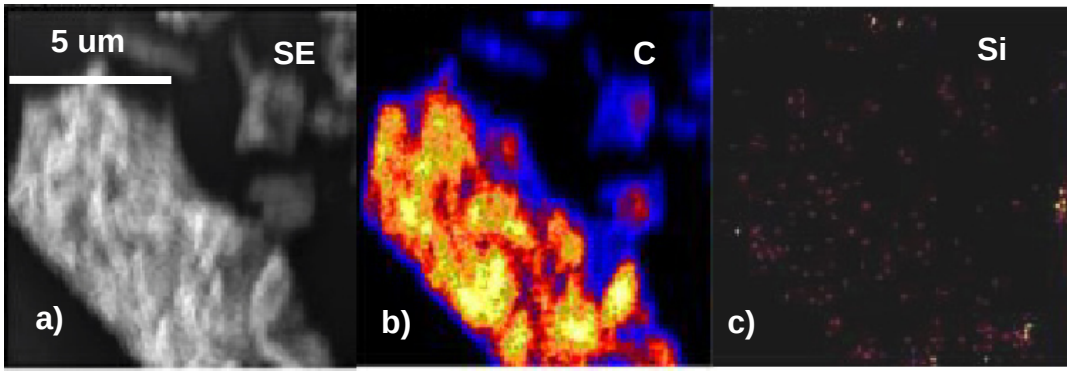


**Figure 6.** a) A secondary electron (SE) image of HF-treated peptidoglycan particles. Note that b) carbon is widely distributed, but c) Si is nearly absent in the sample.

Figure 7 shows individual Si/C ratios determined for each raster plane. Note the lower overall ratio even over 150 sputter planes. However, a steady, but not dramatic increase in Si/C ratio is also noted in this sample, similar to the $SiO_2$ adsorbed material. However, the arithmetic mean Si/C ratios calculated from all the raster planes analyzed yield a value of $5.7 \times 10^{-4} \pm 3.1 \times 10^{-4}$ (Table 2). Assuming carbon is 50% by weight in the peptidoglycan, this suggests a Si concentration ~300 ppm. The difference in measured Si concentration between the HF-treated peptidoglycan and the $SiO_2$ adsorbed sample is nearly 1700 ppm and indicates the peptidoglycan has a weak affinity to the material in aqueous media.

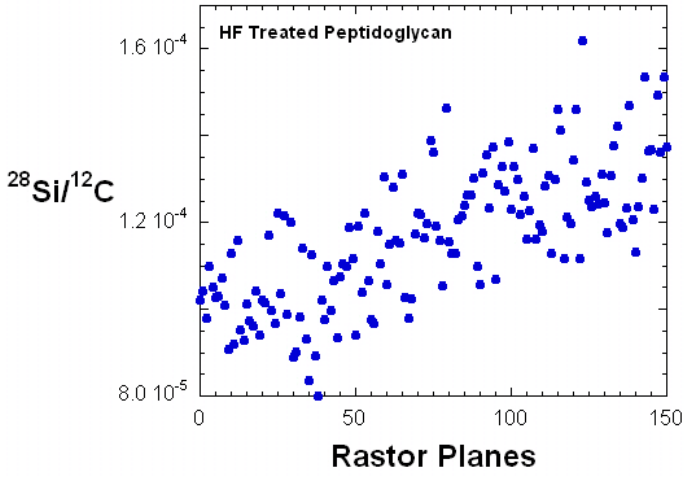


Figure 7. Si/C ratios of the HF-treated peptdoglycan are distinctly lower than the $SiO_2$ adsorbed sample, but a progressive increase is still observed.

POLYACRYLIC ACID

Following the preparation and analysis of the peptidoglycan, an additional material was sought that could provide a more uniform and reproducible Si count in an organic substrate, and have a wider concentration range. Because we were already working with aqueous solutions of $SiO_2$, an attempt was made to isolate $SiO_2$ in a water soluble resin deposited as a thin film. Polyacrylic acid resin was selected because of its water soluble character, relatively low viscosity, and it dries quickly. Therefore, experiments were performed, whereby three equal volumes of polyacrylic acid resin (Polycrylic® by Tompson Miniwax Co.) aliquoted into individual 20 ml glass vials were spiked with different concentrations of dissolved $SiO_2$. The three resulting mixtures contained, respectively, 0.1, 1.1, and 11.4 mg/L of $SiO_2$. A small volume of each was aliquoted onto a glass plate and gently dried under a stream of $N_2$ gas. As a dried film the concentration of Si was 0.3, 3.2, and 32.2 mg/kg, based on a measured polyacrylic acid density of 1.5 g/cc. After drying, each thin film was peeled up from the glass and cut to size for the NanoSims holder with the glass side of the film facing up to provide the flattest surface. An additional film without $SiO_2$ added was also made by the same method in order to evaluate the Si blank levels in this material.

**Table 3.** Results from polyacrylic acid spiked with aqueous $SiO_2$.

| **Concentration** | **$^{28}Si/^{12}C$ ratio ($\times 10^{-5}$)** | **$^{28}Si/^{12}C$ std dev. ($\times 10^{-5}$)** |
|---|---|---|
| **32.2 ppm** | 8.26 | 4.28 |
| | 4.86 | 4.44 |
| | 2.36 | 0.37 |
| | 5.77 | 5.02 |
| | 2.37 | 0.18 |
| | 51.6 | 56.3 |
| | | |
| **3.2 ppm** | 1.66 | 0.18 |
| | 1.23 | 0.17 |
| | | |
| **0.3 ppm** | 4.45 | 4.44 |
| | 3.05 | 2.54 |
| | 2.57 | 2.11 |
| | | |
| **Polyacrylic blank** | 0.83 | 0.31 |

Results of each thin film are presented in Table 3. With the exception of the blank, each different thin film sample was measured on more than one spot. Raster size was 2um for each spot and analyzed between 10 and 50 individual planes. Two observations of note are apparent from the data. Firstly, note that the standard deviation of each analysis is relatively high with the exception of two spots analyzed on the highest concentration sample. This indicates that the Si

counts varied significantly for each spot. Secondly, the 32.2 ppm concentration sample did not have a Si count ten times as great as the 3.2 ppm sample except for one spot. It is plausible that the 3.2 ppm sample represents instrument detection limits. However, the single spot analyzed on the blank sample suggests that the instrument was detecting Si counts an order of magnitude lower than the 1.6 ppm sample. Assuming that this blank analysis is representative of the entire polyacrylic acid, then the inconsistent Si counts for the other samples indicates Si was not homogeneously distributed in the sample. This would also be consistent with the high standard deviation in the analyses.

On further inspection of the 32.2 ppm sample, several spot analyses indicates large variability in the Si/C ratio with depth in the material (Figure 8). In three out of the six spots analyzed the Si/C ratio was more than ten times higher the first half of the analysis compared to the latter half. For those that showed consistent Si/C ratios throughout the analysis, the ratio approximated the expected concentration of ~30 ppm.

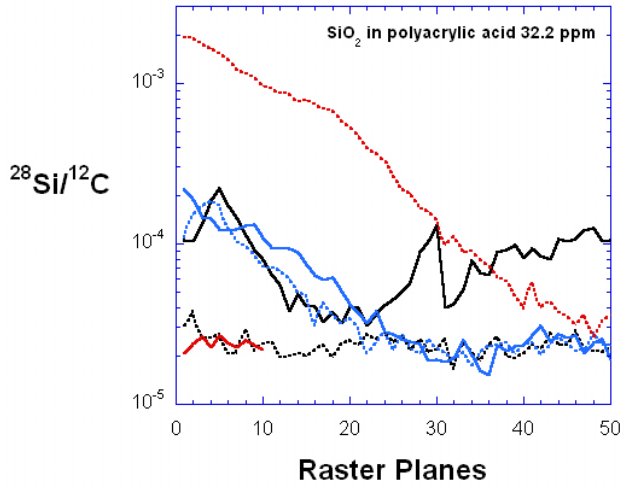


**Figure 8**. Si/C ratios from the six spots analyzed on the 32.2 ppm $SiO_2$ polyacrylic acid thin film indicate Si was not homogeneously distributed for half of them, whereas the remainder yielded ratios nearly same as the lower concentration sample (see Table 3)

The image in Figure 9 illustrates the spatial distribution of Si observed in some of the 32.2 ppm samples spots. Note that the Si is confined to a narrow spot and is largely absent in the surrounding region. This suggests that the aqueous $SiO_2$ spike added to the polyacrylic acid did not homogeneously distribute in the thin film during the drying process. Reasons for this result are discussed later.

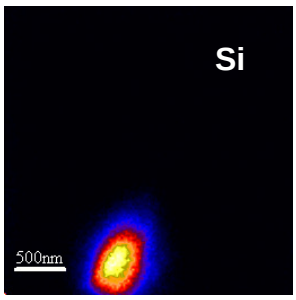


**Figure 9**. Si counts in this 2um spot of 32.2 ppm polyacrylic acid are isolated to a single spot, suggesting incompatibility between the $SiO_2$ and the polymer.

POLYMETHACRYLATE

As a follow-up experiment on developing a Si standard using a polymer, it was hypothesized that a methylated form of Si combined with a hydrophobic polymer resin would result in a more uniform distribution of Si in a thin film. The polymer chosen was a polyisobutylmethacrylate. This was initially dissolved in methylene chloride before preparing thin films. While dissolved, three different volume additions of chlorotrimethylsilane were added to the polyisobutylmethcrylate to create final concentrations in the thin film of 1%, 100ppm, and 1ppm Si. The dissolved material was pipetted onto a ~0.5 cm diameter aluminum bullet to form a dried thin layer of polymer. These were subsequently gold-coated before mounting in a NanoSims holder. Sample analysis spots were sputtered for an adequate time to attain steady Si and C counts.

Figure 10 below shows the results from chained analyses on each sample. Data from each spot analyzed has been numerically averaged to produce the combined plot. Included in the figure is an analysis of a single spot of a polyisobutylmethacrylate thin film prepared in the absence of the chlorotrimethylsilane to determine sample blank levels for Si.

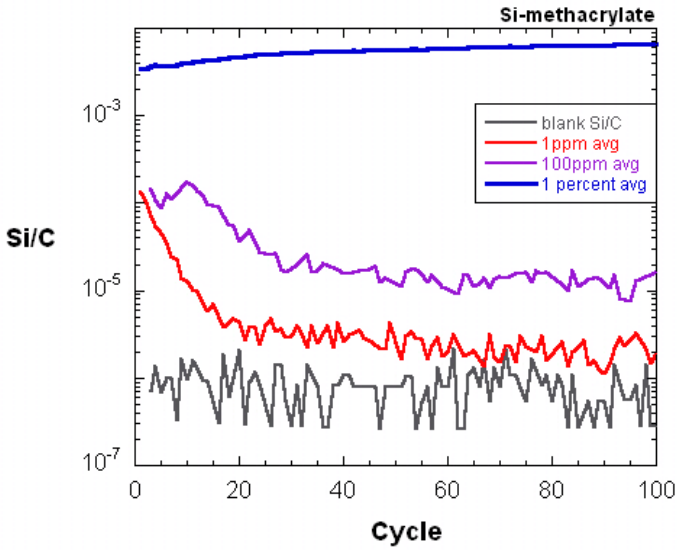


**Figure 10**. Average concentrations of Si (as chlorotrimethylsilane) in polyisobutylmethacrylate thin film. At the highest concentration the Si/C ratio appears uniform after sufficient sputtering and approaches 0.7%, whereas the lower concentrations indicate inhomogeneity with raster depth.

The 1% concentration sample shows a typical progression of increasing Si/C ratios as the sample is rastered over numerous cycles. The trend in Si/C ratio appears to level off at approximately 0.007, which suggests a Si concentration closer to 0.7% although an independent bulk measurement has not been conducted. Samples prepared with the 100 ppm and one ppm Si equivalents

show a distinctly different trend than the 1% sample. In particular, the lower concentration samples indicate a significantly high Si/C ratio in the first 20 planes of analysis.

Table 4 tabulates numerical averages for the Si/C ratio for each analysis spot. These averages were calculated from each raster plane and no planes were manually subtracted. Hence, the 1% sample for instance shows an average value of approximately 0.5% because the low Si/C ratios of the initial planes were included in the averaging. Nevertheless, Table 4 does give an indication of acceptable reproducibility from one analysis spot to the next for the 1% sample. Some significant variation is noted for the 100 ppm and one ppm samples, but these are due to the presence or absence of high Si/C ratios in the earlier raster planes (see Figure 10).

**Table 4.** Si/C ratios of polyisobutylmethacrylate thin films

| **Concentration Si** | **$^{28}Si/^{12}C$ ratio ($\times 10^{-6}$)** | **$^{28}Si/^{12}C$ std dev. ($\times 10^{-6}$)** |
|---|---|---|
| **10000 ppm** | 5612 | 47.3 |
| | 5804 | 50.5 |
| | 5357 | 47.1 |
| | 5344 | 47.1 |
| | 5591 | 48.0 |
| | 5341 | 46.9 |
| | | |
| **100 ppm** | 11.13 | 6.19 |
| | 13.15 | 10.8 |
| | 28.4 | 10.5 |
| | 33.0 | 11.0 |
| | 44.3 | 15.1 |
| | 39.9 | 14.0 |
| | 46.0 | 16.1 |
| | 40.2 | 15.5 |
| | | |
| **1 ppm** | 8.86 | 1.97 |
| | 9.13 | 1.93 |
| | 8.93 | 1.81 |
| | 4.47 | 1.34 |
| | | |
| **polyisobutylmethacrylate blank** | 0.75 | 0.41 |

## MOLYBDENUM

Because molybdenum in biological samples are typically less than 100 ppm, a low abundance molybdenum standard is needed instead to test instrument linearity over a wide concentration range, similar to the approached used for silicon. Furthermore, molybdenum will always likely be in low abundance in biological samples, and therefore it is even more advantageous to create a number of standards in an organic matrix having a concentration range similar to unknowns (e.g., 100 ppb to 100 ppm). Molybdenum is a transition metal and offers a greater possibility of being uniformly distributed at low concentrations in organic polymers. Unlike silicon and other non-metals, transition elements like molybdenum have a high affinity to electron-donating functional polymers, such as those rich in carboxylic acids, and have a good chance of coordinating with terminal hydroxyl groups. In addition, molybdenum is known to strongly adsorb to natural organic materials such as humic acid (also rich in carboxylic acids), or in adsorption media such as activate carbon. Based on this knowledge, procedures were developed to create thin film deposits of low abundance molybdenum standards and also to developed particle-based material with molybdenum as an adsorbed phase. Below are outlined steps for their preparation steps and initial NanoSIMS analytical results. All solutions were measured for molybdenum concentration during sample preparation using the potassium thiocyanate and stannous chloride colorimetric method (Standard Methods, 2005).

### HUMIC ACID

Humic acid is a functional name given to a mixture of organic compounds isolated from natural organic matter in soil, water and some geologic materials using an alkaline extraction/acid precipitation procedure (Stevenson, 1994). Root zone depths in soil typical retain the highest humic acid content in the environment, although humic acids can also be extracted in abundance from coal and peat deposits. River and ocean water tend to be poor in humic acids, but can have high content of lower molecular weight organic material. For this work, an archived humic acid was used that was prepared from a soil in the Livermore area following procedures outlined in Appendix 3.

Humic acids are soluble at pH greater than ~9, which provided a means to mix an aqueous solution of molybdenum with the dissolved humic acid. Aqueous standards of Mo(VI) were prepared by serial dilution of a stock solution of dissolved ammonium molybdate tetrahydrate. For the humic acid adsorption a 42 ml aliquot of 720 mg/L Mo(VI) solution was mixed with the 30 mg of humic acid and fully dissolved with 0.4 ml of 3M NaOH. This resulted in nearly equal Mo(VI) (30.2 mg) and humic acid (30.0 mg) weights. After a few minutes of equilibration time, 0.8 ml of 6M HCl was added until the pH was less than 2. This resulted in re-precipitation of the humic acid, and it was assumed that Mo(VI) was uniformly coordinated at the nano-scale. The Mo(VI) concentration in solution was measured after all the humic acid precipitated, yielding 673 mg/L after accounting for all volume additions, or 29.1 mg Mo(VI) was left in solution. Therefore, the Mo(VI) loss to the precipitated humic acid equaled 1.1 mg and produced a weight

percent Mo(VI) of 3.5% relative to the humic acid. The precipitate was isolated by centrifugation, rinsed twice with methanol, which yielded a total of 0.04 mg Mo(VI) back into solution, and then the precipitate was freeze-dried. NanoSims samples were prepared by simply tapping a small amount of the precipitate onto an aluminum bullet with a scribing tool.

Several NanoSims images were collected for the molybdenum/humic acid sample with the intent of determining the homogeneity of molybdenum distribution at the nano-scale and to obtain an analytical ratio of molybdenum isotopic species to a reference element such as carbon. Figure 11 illustrates the $^{92}$Mo and $^{98}$Mo data collected on one spot of the humic acid sample. At this concentration the molybdenum shows a uniform distribution. The figure also indicates that the $^{92}$Mo/$^{98}$Mo ratio appears consistent throughout the image. Comparative analysis among four different spots on this sample indicates that the $^{92}$Mo/$^{98}$Mo ratio was consistent and averaged 0.6212 ±0.0038, which compares well with the natural abundance ratio of 0.6141.

Significant variation was observed in the Mo/C ratio with analysis depth in the humic acid preparation. Ratios of $^{98}$Mo/$^{12}$C varied from 3.5 to 11.1, and averaged for all analysis spots at 7.64 ±1.87. The highest ratios typically occurred at greater depths. These ratios are further discussed in the context of a relative sensitivity factor (RSF) in the Discussion section below.

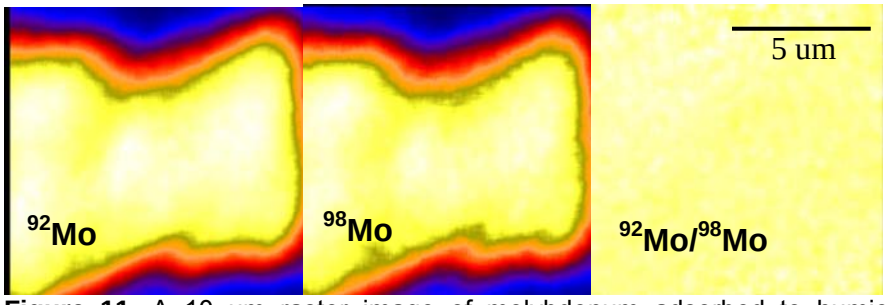


**Figure 11.** A 10 um raster image of molybdenum adsorbed to humic acid at approximately 3.5 percent. Note the homogeneous distribution of the $^{92}$Mo, $^{98}$Mo, and their ratio.

It is also useful to illustrate results from a blank humic acid preparation that ostensibly should be very low or free of molybdenum. Results are shown for one analysis location in Figure 12. Note that that the $^{92}$Mo and $^{98}$Mo appear not to co-vary in the sample, and their ratio shows significant variation across the image. This variability was consistently observed throughout several analysis spots in this sample. Such variation suggests significant interfering masses overlap with the m/z = 92 and 98 region, which will present some complexity in analysis of low abundance standards using the humic acid material. Potential interfering masses and their resolution are discussed below.

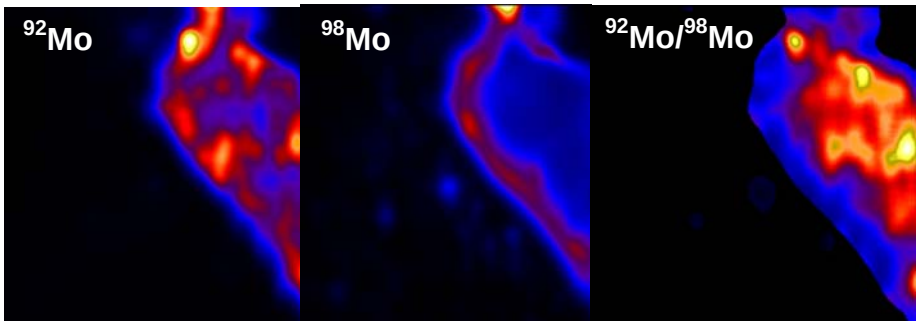


**Figure 12.** A 40um raster of molybdenum in blank humic acid where no additional molybdenum has been adsorbed. Note the distinct difference between the $^{92}$Mo and $^{98}$Mo distributions as well as the heterogeneity in their ratio, indicating significant mass interferences.

## POLYACRYLIC ACID

Applying the same thin film method used for $SiO_2$ above, thin films of Mo(VI) were prepared using the same procedures. In this case standards comprising 102 ppm and 10.2 ppm were prepared along with a blank. It was anticipated that the Mo(VI) would coordinate with free hydroxyl groups in the polyacrylic acid and form a uniform distribution at the nano-scale. Only the results of the 102 ppm sample are presented.

Results for a chained analysis measured for 100 cycles on each 10 um raster are shown in Table 5. Monitored isotopes $^{92}$Mo and $^{98}$Mo show consistent ratios for each analysis spot. Also note that the $^{98}$Mo/$^{12}$C ratios are also very consistent, and the low standard deviation for each illustrates uniformity of the molybdenum with depth in the polyacrylic acid. These ratios in relation to RSFs will be discussed further below.

**Table 5.** Results of polyacrylic acid with 102 ppm molybdenum

| $^{92}$Mo/$^{98}$Mo ratio | $^{98}$Mo/$^{12}$C ratio | $^{98}$Mo/$^{12}$C std dev |
|---|---|---|
| 0.607 | 0.0229 | 0.0003 |
| 0.601 | 0.0211 | 0.0007 |
| 0.601 | 0.0213 | 0.0007 |
| 0.597 | 0.0224 | 0.0008 |
| 0.599 | 0.0228 | 0.0008 |
| 0.601 | 0.0225 | 0.0008 |
| 0.605 | 0.0229 | 0.0009 |
| 0.601 | 0.0234 | 0.0009 |

## CALCIUM

A set of organic Ca standard were made as a polyacrylic acid thin film. The preparation of Ca, as well as other aqueous elements, requires not introducing additional elements to the matrix that may cause unwanted mass interferences. Therefore, we consider it critical that all elements prepared by this method use an organic acid form. Therefore, a calcium acetate was prepared by mixing an excess of $Ca(OH)_2$ with glacial acetic acid, followed by stirring and warming for a couple hours. This solution was filtered and the filtrate was crystallized to a Ca-acetate salt. An aliquot of this salt was weighed and dissolved in polyacrylic acid resin (Aldrich; molecular weight ~2000) to form a 1% by weight thin film when dried.

## STRONTIUM AND BARIUM

These elements were prepared by the same polyacrylic acid method as the Ca above. In the case of Sr, a $Sr(Cl)_2$ solution was added to a $NaCO_3$ solution adjusted to pH~11 using NaOH that formed an insoluble $SrCO_3$. The $SrCO_3$ was isolated by centrifugation, followed by dissolution into glacial acetic acid. The resulting Sr-acetate was mixed with polyacrylic acid resin to form thin films as outlined above. The same method was employed for Ba except that the starting material was $BaCO_3$, which as dissolved in the glacial acetic acid.

## CHLORINE

POLYVINYL CHLORIDE (PVC)

Food-grade PVC tubing (VWR® Clear, Flexible Tubing #89068-536) was prepared for a NanoSims sample by manually slicing a thin layer of tubing material, gold coating, and mounting in a NanoSims holder. A total of 6 individual 5 um analyses were performed using a Cs+ primary beam and collecting the $^{35}Cl$ and $^{12}C$ secondary ions. Reasonably consistent ion counts were collected for each spot over ~30 minutes each. Mean $^{35}Cl/^{12}C$ ratios were calculated to be $3.7x10^{-2}$ $\pm 6.3x10^{-4}$.

A separate sample was prepared for electron probe analysis to perform an independent Cl concentration measurement. This analysis resulted in 20.9% ±1.8% mass percent Cl for the tubing material. Note that for this concentration the expected $^{35}Cl/^{12}C$ ratio would be around 0.4 for a standard PVC polymer formula. This suggests that significant mass fractionation occurs between chlorine and carbon from organic substrates. This is discussed further below.

## FLUORINE

TEFLON

A sample of polytetrafluoroethylene (PTFE) was prepared for a NanoSims analysis. The sample was gold coated before analysis, but it was anticipated that there was a high potential of the sample acting as an insulator. This is because PTFE has one of the highest surface resistivities ($>10^{-17}$ ohm/cm$^2$) of all polymers

and is commonly used as an insulator for electronic components. A single analysis proved this correct. Initial sputtering yielded high counts of both carbon and fluorine, but after a couple minutes counts diminished rapidly. A real-time image of secondary electrons revealed that the raster area was absent of secondary electrons due to charge build-up. Consequently, this material was abandoned as a potential fluorine standard.

## IMPLANTATION

A fluorine implant was made in the lab of Wilson, Hughes Research Lab, Santa Barbara, CA. Epoxy blocks were used as the organic matrix. The F-implanting used a 200 kiloelectronvolt source emitting a fluence of $1.2e^{14}$ atoms/$cm^2$. These parameters were chosen so that the maximum concentration at depth did not exceed 1000 ppm F, at which level damage to the epoxy could affect the measurements but would be above background levels. Multiple analyses were conducted on the implant using a 4 um raster area and analyzed for ~45 minutes at each spot (i.e., 100 individual planes of data). Figure 13 is an example of one analysis spot on the F-implant. The data show that the implantation parameters resulted in a successful implant for quantification.

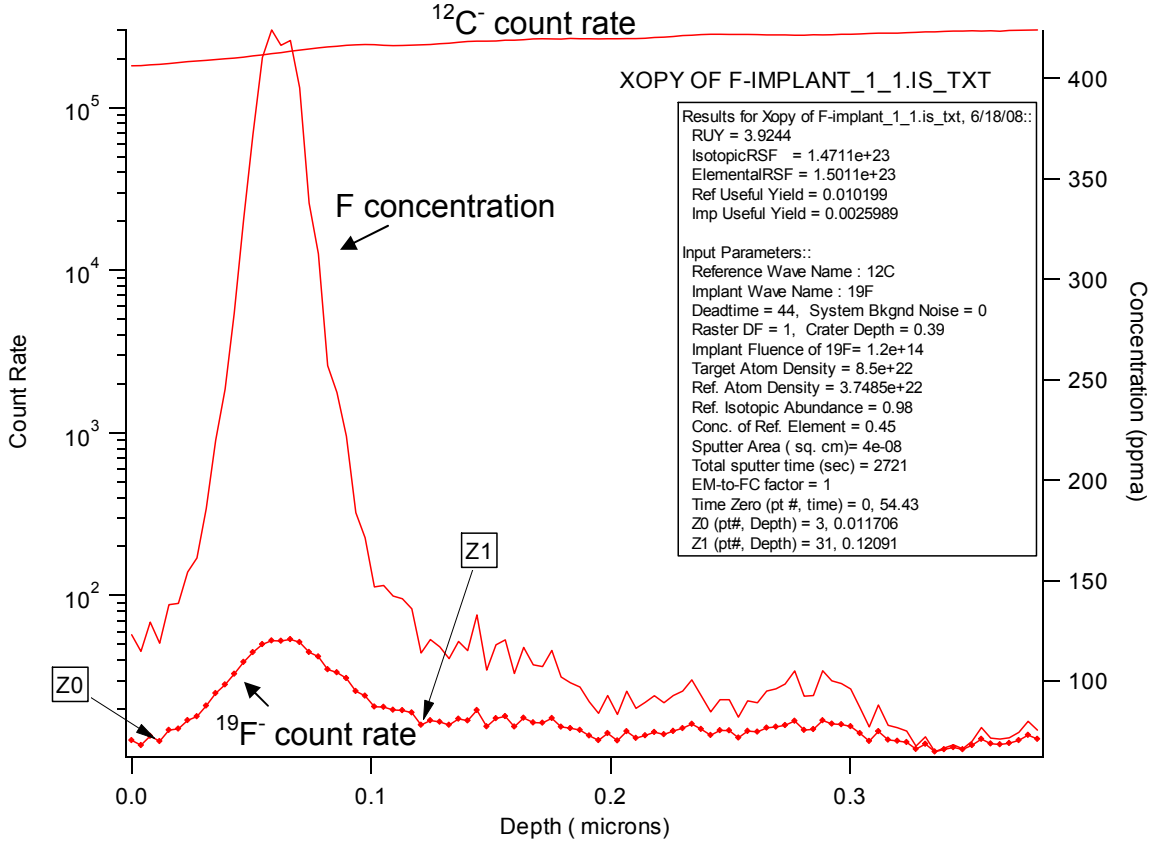


**Figure 13**. Depth profile of F implant in epoxy, showing the F and C count rates, and the depth resolved concentration of F.

Post-processing of the raw F data used custom LLNL software (RUYGeneric), which computes the implant concentration with depth and a relative useful yield (RUY). RUY is equivalent to relative sensitivity factor, but independent of the specific elemental isotope abundances (Phinney, 2006). Input parameters to the computation are raw data for a major element in the epoxy matrix (C in our case), the major element's atom density in the epoxy, and the raster area crater depth.

## DISCUSSION

Standardizing quantitative analysis for an instrument system relies on measuring a known amount of an element in a sample type reasonably similar to the sample of interest. Most commonly used is an external standardization approach whereby samples are created and they contain element of interest at different concentrations, and these are measured in the instrument to produce a calibration curve. In addition, a sample absent of the element is prepared for testing instrument blank. However, to increase the rigor of this calibration, additional samples are created compositionally similar to the samples of interest in order to test instrument performance against the sample matrix both with and without the element. This may require a significant effort if the composition of the sample of interest is complex and largely unknown.

The analytical method of secondary ion mass spectrometry (SIMS) has been present in science and technology research and development for many decades. As this instrumentation evolved, specific research endeavors demanded quantitative analysis. For example, the rise of the semiconductor industry created a need for minor and trace element analysis at micrometer spatial scales in solid materials. Quantitative analysis primarily utilized ion implant methods, which provided a means to precisely control specific ion fluence accelerated and bombarded on a material target compositionally the same as the material of interest. The material bombardment created an external standard with a known element quantity that when analyzed by SIMS provided a quantitative measure of the instrument's performance with respect to ionization and detection efficiency. It furthermore helped map the relative differences in ionization potential among various elements from the same substrate. Methods evolved to normalize these potentials into relative sensitivity factors (RSF; Wilson et al., 1989), or a parameter independent of isotope abundance such as relative useful yield (RUY; Phinney, 2006). Unfortunately, ion implantation can be expensive and time consuming considering that beyond Si-wafers there are many various materials and elements potentially needing a similar rigorous quantitative examination. Consequently, independent bulk analysis of the material of interest can be equally applied instead, particularly since elemental analysis by inductively-coupled plasma mass spectrometry (ICP-MS) has become a routine analytical technique. The drawback of this alternative is that an independent effort is needed to quantitatively convert solid material into a dissolved state and guarantee substantial recovery of the elements of interest. However, solely relying on ICP-MS for all quantitative verification ignores the opportunity to better

understand an instrument's performance for various samples and evolve toward external and internal standards used only for SIMS.

NanoSIMS is the latest generation of SIMS instruments and its coaxial optical design is ideally suited to analyze sub-micron fields of biological material, although its application easily extends into various sample types (e.g., McKeegan, et al., 2006; Oehler et al., 2006; Hermann et al., 2007). The multi-collection detection scheme further provides simultaneous analysis of multiple elements from a single pixel region being sputtered. Although isotopic ratios of these multi-collected ions reflects the major elemental concentration ratios (e.g., Hallegot et al., 2004), several issues introduce uncertainty into quantitative results for lower abundant species. Chief among these are the differential ionization potential of elements from the specific substrate. In biological applications carbon is the most relevant ion to use for normalizing other elemental ions, yet carbon ion yields are several orders of magnitude higher using a $Cs^+$ versus an $O^-$ primary sputtering source. Examination of transition elements in biological material in most cases requires an $O^-$ primary source, which more efficiently produces metals ions than carbon. Consequently, RSFs need to be determined and applied in order to produce quantitative results. Currently, the only extensive RSF database is for implants in silicon substrates, although some elements are also characterized for diamond (Wilson et al., 1989). Other factors affecting ion ratio yields can be related to instrument tuning and uncertainties in sputtering rates, transfer efficiencies of secondary ions, and diffusional migration of elements within the material during the sputtering process. All these factors point to the need for development of external standards specific to biological applications.

It should be noted that several studies using NanoSIMS analyzed samples from biologically-mediated isotope enrichment experiments and documented preferred transport and accumulation at the sub-cellular level (e.g., Kleinfeld et al. 2004; Lechene et al., 2006). Comparison of enriched isotopic ratios to the natural abundances in non-isotopically enriched controls provides a means to derive enrichment factors and material transport (Lechene et al., 2006). Extending isotopically enriched analysis into abiotic organic materials also requires the rigor of creating external isotopic standards and calibration curves (Kraft et al., 2006).

The successful development of external standards applied to various NanoSIMS quantitative analysis requires achieving three key steps that involve 1) obtaining element uniformity at the nano-scale in an organic matrix, or achieving a heterogeneous distribution that can be analytically repeated, 2) producing a material that has a similar concentration range of elements as the sample, and 3) demonstrating that the RSFs for the standard are the same as the sample. It would be furthermore advantageous to create standards that can also be modified to introduce potentially interfering elements in order to map out and resolve low abundances (low ppm to high ppb) of elements of interest.

## Discussion of Natural Materials

NanoSims results from the preparation and analysis of colloidal material indicate that low concentrations of $SiO_2$ can be introduced into them, but that the distribution within a particle and between particles is significantly heterogeneous. In the case of $SiO_2$, intra-particle variation was measured to greater than a factor of hundred (see Fig. 5), whereas inter-particle variation was greater than a factor of four. This variability was observed in a fairly purified material such as peptidoglycan that was equilibrated with a $SiO_2$ solution passively using a dialysis membrane. The heterogeneity suggests that molecular $SiO_2$ may not be simply adsorbed to active sites in a uniform distribution, but possibly are forming areas of localized high concentration. Furthermore, simple $SiO_2$ monomers may not be the main $SiO_2$ molecular form interacting with the peptidoglycan. Oligomers could also be actively binding with the peptidoglycan or alternatively forming from a monomer-organic colloid interaction that initiates polymerization.

Peptidoglycan is polymerized glucose-monomers alternating with ring substitutions of n-acetyl groups. In situ, the terminal hydroxyls form important linkages to proteins and phospholipids representing the functional components of individual cellular activity, whereas the glucose-structure forms a rigid barrier for cellular integrity and to modulate transport in and out of the cell. Extraction and purification of peptidoglycan usually hydrolyzes the hydroxyl linkages, resulting in the basic structure shown below.

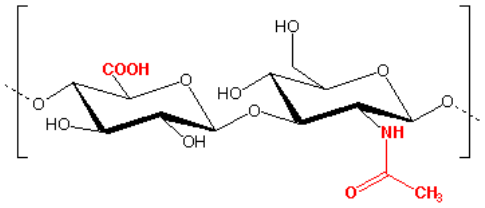


D-glucuronate N-acetyl-D-glucosamine

It is anticipated that the $SiO_2$ is primarily interacting with the amide group, since terminal hydroxyl will have similarly negative charge states as the $SiO_2$, whereas the amide is likely protonated, particularly at lower pH. Although equilibration experiments at low pH were not performed for this initial work, other evidence suggest greater interaction is expected. For example, recent works investigating $SiO_2$ polymerization in diatom tests indicate terminal amines in select proteins promote ionic interaction with $SiO_2$ monomers and the formation of $SiO_2$ nanospheres (Kroger et al., 1999). This interaction has stimulated other investigations to document the amino-containing peptide influences on the polymerization of $SiO_2$ sol-gels (Coradin et al., 2002). It was recognized that the peptide chain length controls rates of $SiO_2$ gelation, oligomers are sequestered during this process, and that initial adsorption promotes a polyelectrolyte-driven gelation process. Similar effects have been noted for other amino-containing polyelectrolytes (e.g., Chang et al., 2006; Demadis and Neofotistou, 2007). It should also be noted that biosilification processes under investigation in plants

also show evidence of Si-induced biological defense and active Si-transporters for promoting abiotic accumulation (see Currie and Perry, 2007 for review). Accumulated evidence thus far suggests that $SiO_2$ in biological systems, and its interaction with key regulating organic constituents, is bioconcentrated rather than homogeneously distributed. This evidence suggests that specific proteins with terminal amines are responsible for this process. Consequently, it is not surprising that the $SiO_2$ distribution was heterogeneous in peptidoglycan used for our experiments. Even though the peptidoglycan is largely absent of terminal amines, the amide function likely is a point of $SiO_2$ interaction instead. If the amide-$SiO_2$ (monomer or oligomer) interaction is ionic, than this may promote limited $SiO_2$ polymerization and cause localized high concentrations of Si relative to carbon in final colloid preparation. It can be seen that significant increases of Si/C ratios are observed for all the peptiodoglycan spots analyzed in Figure 5. This increase may represent polymerized $SiO_2$ localized in the core of the particle and surrounded by peptiodoglycan. This model is consistent with gelation processes observed for terminal amines in other works (Coradin and Livage, 2001; Coradin et al., 2002).

However, at this point alternative explanations cannot be ruled out. For instance, the large size of the peptidoglycan molecule will inevitably fold in various shapes during the sample process, leading to a complex tertiary molecular structure. Furthermore, the peptidogycan was initially dispersed in a saline solution before interacting with the $SiO_2$ solution. Freeze-drying invariably led to dehydration reactions that would likely promote electronic repulsion between $SiO_2$ and terminal hydroxyls, which could lead to zonation of $SiO_2$ surrounded by peptiodoglycan. This might have also promoted limited polymerization of $SiO_2$.

Ultimately, the preparation and use of the peptidoglycan or the organic colloids as standards will need to demonstrate a consistent SiO2 concentration that is reasonably close to those of samples being analyzed. Given the large variation within a single particle, and the lesser but significant difference between particles, it can be concluded that use of these materials for standards will require analysis of enough spots so that an average value of the material is achieved. This initial work only analyzed a limited number of spots, but follow-up work is planned. The analysis approach for standardization would need to be essentially identical as that currently used for individual analysis of spores by NanoSims, which entails collecting enough individual spot analysis to create a statistical representation of quantitative elemental distribution. Verification can be made with careful bulk analysis of the material (and the spores) using methods of sample digestion followed by ICP-OES. Currently, these methods are being developed and will be implemented on a routine basis for future standards development. Further work may be need on the material preparation approach. For instance, NanoSims measurements of the peptiodoglycan sampled directly from the reagent bottle (data not presented) indicated $SiO_2$ content greater than the hydrofluoric acid treated sample (Table 2). Pretreatment with dilute hydrofluoric acid beforehand to extract as much $SiO_2$ from the material as

possible before re-equilibration with a $SiO_2$ solution might reduce the occurrence of high Si/C ratio zones observed in the current preparation. However, results from the organic colloid preparation (Table 1), which underwent a hydrofluoric acid treatment, suggest that $SiO_2$ has a preference to concentrate in these materials. Nevertheless, influence of humic material associated with the peptidoglycan of the organic colloids may enhance zonation or polymerization of the $SiO_2$ because of the high density of terminal carboxyl groups common in humic materials.

Molybdenum adsorption to humic acid also resulted in a heterogeneous distribution, as noted by large variability in Mo/C ratios on individual spots. The homogeneous isotopic ratio rules out any possibility from interfering masses. The variation is not as great as observed for $SiO_2$, however, it is large enough to suggest that the preparation method results in the distribution. It is possible that the tertiary structure of the humic-molybdenum complex after freeze-drying has promoted a confirmation favoring molybdenum zonation. In this case, the electronic state of complexed molybdenum atoms would have to contrast with the remaining portions of the humic material and cause complex folding of the final structure. However, it is just as likely that the humic material is heterogeneous, and only portions of it complex molybdenum and segregate from the remainder. Molecular heterogeneity has long been recognized in humic material (e.g., Stevenson, 1994). Its preparation as a base extractable only represents those organic substances in soil that have ionizable functional groups at high pH. Condensation of the humic acid at low pH may draw out non-condensible substances by simple hydrophobic interaction, rather than remaining in solution. Nevertheless, the heterogeneity of the Mo/C ratio does indicate that a similar analysis of multiple spots is required for this material as well if it is to be used as a standard.

Regardless of the heterogeneity in molybdenum, it is important to begin to understand the relative sensitivity of molybdenum ionization compared to carbon in organic substances, and further compare that to known sensitivities in Si-wafer. The humic acid preparation can be assumed to contain 50% carbon by weight, since most humic substances range between 40 and 60% carbon (Thurman, 1984). Using the 3.5 weight percent calculated early, this would lead to an estimated Mo/C ratio of $7.1 \times 10^{-2}$. Molybdenum has 7 stable isotopes, and NanoSims data measured those of m/z of 92 and 98, which have natural abundances of 14.8 and 24.1%, respectively. Furthermore, carbon has two stable isotopes of 12 and 13, and we assume 98% comprises $^{12}C$. Using $^{98}Mo$ in our estimate would result in a predicted $^{98}Mo/^{12}C$ for the humic acid preparation of $1.7 \times 10^{-2}$. NanoSims secondary ion images were collected by sputtering with an $O^-$ primary beam. For implanted Si-wafer using a $O_2^+$ primary beam, the RSF for carbon is approximately 300 times greater than for molybdenum (carbon ionizes poorer), and the relative difference in RSFs for $^{12}C$ and $^{98}Mo$ is 1316 (Wilson et al., 1989). Assuming for the moment that these same ionization potentials apply for organic material, a $^{98}Mo/^{12}C$ ratio predicted for a NanoSims

analysis of the humic acid preparation would be ~22. However, of the humic acid sample spots analyzed, the average was instead 7.64 ±1.87. This difference would suggest that the relative RSFs for molybdenum and carbon in this organic material are a factor of 2.9 lower than reported in an implanted Si-wafer.

Significant interferences were observed in the NanoSims analysis of blank humic acid, which was not equilibrated with the molybdenum solution (Fig. 12). Similar interferences were also observed for untreated NIST standards SRM 8414 - Bovine Muscle and SRM 1577b - Bovine Liver (data not shown). These reference materials have 3.5 ppm and 0.08 ppm molybdenum concentration, respectively, yet their $^{98}Mo/^{92}Mo$ show significant deviation from natural abundance. For humic acid the molybdenum concentration is not yet available, but a low ppm to low ppb concentration is anticipated (e.g., Bibak and Borggaard, 1994). In order to understand the potential interfering ions at m/z 92 and 98, molecular cluster analysis was performed by comparing the mass difference between abundant elemental isotopes in the humic acid and the $^{92}Mo$ and $^{98}Mo$. The mass difference and required mass resolving power to analytically detect molybdenum only are defined as

$$Resolving\ Power = \frac{m_1}{(m_1 - m_2)}$$

where $m_1$ is the exact mass of the molybdenum isotope and $m_2$ is the exact mass of the potential interfering cluster, and their simple arithmetic subtraction is the mass difference. For $^{92}Mo$ interferences, a potential candidate element in humic acid would be zirconium, which is known to exist in soils at high ppm concentrations, and $^{92}Zr$ has a 17% natural isotope abundance. Mass difference is ~0.001 amu, which makes it unresolvable with respect to $^{92}Mo$ using NanoSims. Also potentially contributing are the molecular clusters $^{12}C$-$^{40}Ca$-$^{40}Ca$, $^{12}C$-$^{24}Mg$-$^{56}Fe$, $^{24}Mg$-$^{24}Mg$-$^{44}Ca$, and $^{1}H$-$^{12}C$-$^{39}K$-$^{40}Ca$, all the elements of which have high atom abundance in humic acid extracts. However, all these clusters only require mass resolving power <7000. It is anticipated that a resolving power of ~9000-10,000 can be used and still detect enough low abundance molybdenum to achieve quantitative analysis. For $^{98}Mo$ the clusters potentially contributing to interference may be $^{16}O$-$^{26}Mg$-$^{56}Fe$, $^{1}H$-$^{26}Mg$-$^{31}P$-$^{40}Ca$, and $^{1}H$-$^{1}H$-$^{40}Ca$-$^{56}Fe$. Two of these clusters will require resolving power >14,000 in order to analyze $^{98}Mo$ as a separate peak.

For future analysis of molybdenum, it may be necessary to use in addition other stable isotopes. Note all stable isotopes of molybdenum have natural abundances greater than 9%. Table 6 below shows cluster analysis for isotopes that may serve as better detection ions. Note that there are several potential interfering mass clusters that are unresolvable. A method for testing the significance of the clusters is discussed below in relation to polymers.

**Table 6.** Molecular cluster analysis for molybdenum isotopes

| Mass | $10^3$ x ($m_1$-$m_2$) | Abundance | Required Resolving Power |
|---|---|---|---|
| **$^{95}$Mo** | | | |
| $^{39}$K-$^{56}$Fe | -7.2 | 0.8554 | 13199 |
| $^{40}$Ca-$^{55}$Mn | -5.2 | 1.0000 | 18256 |
| $^{12}$C-$^{39}$K-$^{44}$Ca | 13.3 | 0.0192 | 7110 |
| $^{16}$O-$^{39}$K-$^{40}$Ca | 15.4 | 0.9019 | 6174 |
| $^{16}$O-$^{23}$Na-$^{56}$Fe | 13.8 | 0.9150 | 6884 |
| **$^{96}$Mo** | | | |
| $^{40}$Ca-$^{56}$Fe | -7.1 | 0.8891 | 13440 |
| $^{16}$O-$^{40}$Ca-$^{40}$Ca | 15.4 | 0.9375 | 6216 |
| $^{16}$O-$^{24}$Mg-$^{56}$Fe | 10.2 | 0.7228 | 9376 |
| $^{12}$C-$^{40}$Ca-$^{44}$Ca | 13.4 | 0.0200 | 7155 |
| **$^{98}$Mo** | | | |
| $^{42}$Ca-$^{56}$Fe | -11.8 | 0.0059 | 8270 |
| $^{44}$Ca-$^{54}$Fe | -10.3 | 0.0012 | 9502 |
| $^{40}$Ca-$^{58}$Fe | -9.5 | 0.0027 | 10267 |
| $^{16}$O-$^{40}$Ca-$^{42}$Ca | 10.7 | 0.0063 | 9129 |
| $^{16}$O-$^{41}$K-$^{41}$K | 13.2 | 0.0045 | 7441 |
| $^{16}$O-$^{39}$K-$^{43}$Ca | 12.0 | 0.0013 | 8167 |
| $^{16}$O-$^{26}$Mg-$^{56}$Fe | 7.0 | 0.1007 | 13902 |
| **$^{100}$Mo** | | | |
| $^{44}$Ca-$^{56}$Fe | -17.1 | 0.0191 | 5858 |
| $^{12}$C-$^{40}$Ca-$^{48}$Ca | 7.6 | 0.0018 | 13064 |
| $^{12}$C-$^{44}$Ca-$^{44}$Ca | 3.5 | 0.0004 | 28664 |
| $^{12}$C-$^{48}$Ca-$^{40}$Ca | 7.6 | 0.0018 | 13064 |
| $^{16}$O-$^{44}$Ca-$^{40}$Ca | 5.5 | 0.0202 | 18134 |
| $^{16}$O-$^{28}$Si-$^{56}$Fe | -0.7 | 0.8439 | 143834 |
| $^{23}$Na-$^{23}$Na-$^{54}$Fe | 11.7 | 0.0580 | 8557 |
| $^{26}$Mg-$^{26}$Mg-$^{48}$Ca | 10.2 | 0.0000 | 9754 |
| $^{28}$Si-$^{28}$Si-$^{44}$Ca | 1.9 | 0.0177 | 53818 |

## Discussion of Polymers

The polyacrylic acid resin used for this initial investigation was readily soluble in water and miscible with dilute solutions of dissolved ions. The dense carboxylic acid function of the polymer provides a rich electron-donating environment for complexation to inorganic species during the drying process. In the case of molybdenum (VI), donated electrons easily fill unoccupied orbital shells, thus completing complexation. The spatial scale of this process is small enough to ensure uniformity using NanoSims analysis.

### Silicon

For $SiO_2$, complexation in polyacrylic acid was apparently absent. Following the reasoning of electron donation, it can be concluded that the anionic state of

$Si(OH)_4$ in the aqueous solution was incompatible with the electron-rich environment of the polyacrylic acid. As a result, it is likely that the $Si(OH)_4$ migrated towards itself and polymerized, forming the observed nano-scale nodules as illustrated in Figure 9. This interpretation is consistent with the lack of known dehydration reactions between the carbon and silicon centers to form a Si-O-C bond. Such bonding usually requires stronger leaving groups like halogens bonded to the Si or C. It would stand to reason that during the drying process, the $Si(OH)_4$ dehydration reactions were more favorable with other silicon centers, preferring $SiO_2$ polymer formation instead.

Thus forms the basis for why a silane-methacrylate thin film was attempted instead. The polyisobutylmethacrylate used has the following structure:

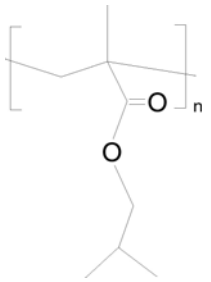


*polyisobutylemethacrylate*

Note that the most reactive point on this molecule is the carbonyl function. In order form a covalent bond with the silane, electron donation would be required from the carbonyl to the silane followed by hydrogenation of the carbon. This reaction may have taken place for the 1% Si sample, since during the drying process bubbling was noted, suggesting evolution of $Cl_2$ gas. Another possibility is that small amounts of water may have been present causing a similar $Cl_2$ evolution. The bubbling was not noted for the lower concentration samples. Nevertheless, the distribution of the Si counts in the final films appears to be consistent with depth for all samples. However, it was the carbon counts that varied over the course of the analysis. For the 1% sample, the carbon reached a maximum early in the analysis, but then steadily decreased, whereas for the low concentration samples the carbon steadily increased over the course of the analysis. This is why the Si/C ratio steadily increased for the 1% sample, but decreased for the lower concentrations.

Several reasons may explain this variability. Among them is an incomplete reaction of the silane with the methacrylate for the low concentration samples, causing phase separation of the two compounds during the drying process. However, that does not explain the apparent consistency in Si counts with depth. In contrast, the 1% sample likely resulted from some transformation during drying that may have change the material property of the final film. This change could have caused the different ionization with depth compared to the low concentration samples.

Given the uncertainty in the reasons for the variability, it is best to concentrate on future approaches that overcome such differences. Consequently, suggestions for future attempts to work with a methacrylate polymer and a silane are to 1) use acetylnitrile as the solvent to reduce possible reaction, 2) use a hydroxyethylmethacrylate resin instead to provide a more readily available electron donator, and 3) react by slow addition and stirring in water-free conditions to promote uniformity in Si substitution. It is hypothesized that this should provide a solution that can be dried to a thin film having a more uniform composition.

Even though the Si/C ratio was inconsistent in the methacrylate samples, the results presented in Figure 10 are encouraging and suggest that little mass fractionation between these two elements occurs at low Si concentration. It is tentatively safe to suggest at this point that the Si/C ratio analyzed in the SiC standard approximates analyzed ratios at lower concentrations. Future work will be required to reduce uncertainty.

Molybdenum

Given the apparent successful results of molybdenum in polyacrylic acid, it is subsequently important to understand the difference in RSF between Mo and C in this material versus others such as the humic acid and Si-wafer. For the 102 ppm sample the expected $^{98}Mo/^{12}C$ ratio with no mass fractionation is $5.0x10^{-5}$. However, the observed average ratio in the sample analyses was 0.0224 ±0.0007. Note this a factor of 446 difference, indicating the preference of Mo ionization over C for the $O^-$ primary source. Applying the ratio of RSFs for $^{98}Mo$ and $^{12}C$ from implanted Si-wafer under $O_2^+$ ionization to the expected secondary ion ratio (i.e., $5.0x10^{-5}$) yields a mass fractionation adjusted ratio of 0.0661. This adjusted ratio compared to that observed is different by a factor of 2.95. Recall that the difference in expected versus observed $^{98}Mo/^{12}C$ ratios for the 3.5 weight percent humic acid was calculated to be 2.9. This suggests that the relative ionization rates of Mo and C are essentially the same between the humic acid and the polyacryilic acid samples. Since humic acid has similar composition to biological systems, it stands to reason that the same relative ionization rate would apply to vegetative and sporylated cells analyzed for molybdenum.

Another advantage of the polyacrylic acid polymer is that many transition elements that can be dissolved in water can be used as a standard. Other transition elements of interest include Ni, Zn, Cr, and Cu, which all have soluble salts. However, there is also need for standardization of P, Al, F, Cl, and I. For the poorer metals and non-metals, polyacrylic is likely not the best choice for a standard material. For elements such as Si and Al, results like those observed in Figure 9 are likely to occur. It is not clear how soluble halogen salts will disperse in the dried polyacrylic acid, but attempts will require using their Na salts and determine if they agglomerate during the drying process. For alkali and alkaline earth metals, the positive charge in aqueous solutions of these elements may

more readily interact with the carboxylic acid groups during dry down and form weak complexation.

The discussion of aqueous salts and polyacrylic acid interaction is also relevant for understanding interfering ions. Recall that large numbers of possible interfering masses potentially mask low abundance molybdenum in biological samples. To map out these potential interferences will require introducing suspect elements into the polyacrylic acid standard. Possible elements include Fe, Ca, K, Mg, and Na. Most of these will need to be introduced at low percent to high ppm concentrations. Creating their soluble salts is trivial in aqueous solution, but in order to eliminate possible new interferences from their complimentary anions, these elements will need to be dissolved as organic acids. All of these elements with the exception of Fe are soluble in acetic acid. Fe is soluble in oxalic acid. Each element needs to be introduced into the acid as a soluble carbonate. Future work will create a group of experimental standards to test the ability to distribute somewhat uniformly these interfering elements into polyacrylic acid, followed by mapping out potential mass interferences.

Chlorine

The PVC tubing used for the NanoSims analysis provided reproducible and consistent $^{35}Cl/^{12}C$ ratios in multiple locations, indicating that this material is a good candidate for a high concentration Cl standard. However, the difference in the average observed $^{35}Cl/^{12}C$ ratio ($3.7x10^{-2}$) and the Cl concentration measured on the electron probe needs to be reconciled. Converting the observed $^{35}Cl/^{12}C$ ratio to a Cl mass concentration assuming that C comprises 38% by mass (i.e., PVC = $C_2H_3Cl$), the observed Cl concentration would be $1.84x10^{-2}$. Note that for C and Cl implanted on Si-wafer and ionized under a Cs+ source, the ratio of their respective RSFs is 0.14, with C more favorably ionized. Accounting for isotopic abundances, the RSF ratio applied as a correction to the observed $^{35}Cl/^{12}C$ would be 0.107. This would result in an adjusted observed $^{35}Cl/^{12}C$ ratio on the NanoSims of 0.345. Adjusting this value to a Cl mass fraction as done above, results in a Cl concentration of 0.17, or 17% by weight. This result is within 20% of the concentration measured on the electron probe. Consequently, the relative mass fractionation of Cl and C measured for implanted Si-wafer appears to approximate that of a PVC polymer.

## SUMMARY

Initial efforts to explore natural and synthetic organic materials as elemental standards for biological investigations using NanoSIMS has provided two important avenues of material utilization. Firstly, in order to mimic the spot analysis approach used for spores, select organic colloids, or nanoparticles, have been manipulated to adsorbed silica and molybdenum. However, element abundance is not uniform at the nano-scale for these materials because the final tertiary molecular structure or limited polymerization prevents simple polymeric-

type of distribution. Nevertheless, this should not prevent developing optimal preparation approaches that result in inter-particle similarity. Achieving this could yield a standard material that when measured over multiple spots produce a calculated average the same as that measured by a bulk analysis approach. Having a standard that performs this way can periodically test the consistency of instrumental tuning over the timeframe of the multi-particle analysis, which is important to demonstrate for the spore analysis. Future work in this area should focus on optimizes the adsorption conditions and expand the material type for non-metal elements that do not readily complex with oxidized functional groups common to natural colloidal material.

Secondly, polymers that can be made easily into thin films may represent an ideal method for developing calibration curve standards. Polyacrylic acid is readily suitable for water soluble transition metals and may also be able to complex alkali and alkaline earth metals. It is not suitable for non-metals such as silicon. For the latter, initial progress is made using silane compounds polymerized to methalcrylate. Although element uniformity was not achieved for this initial work, the approach promises to yield large improvement with future iterations. Nevertheless, with uniform distribution at low abundance levels, element ionization yields relative to more abundant species can be determined in order to delineate mass fractionation effects during sample sputtering. Furthermore, elements that might produce interfering masses during low concentration analysis of metals can be introduced in the standard material to better resolve them.

Additional materials explored during this initial investigation showed mixed results. For high abundance chlorine, PVC appears to provide a suitable standard material. Fluorine may be best analyzed in the near future as an implant sample in epoxy. Its distribution in a polyacrylic acid as a NaF salt should be tested in future work.

## ACKNOWLEDGEMENTS

Funding the Si, Cl, Ca, Sr and Ba work came from the Department of Homeland Security. Funding for the Mo work and the F implant came from LLNL. We thank C. Ramon for technical assistance.

## REFERENCES

Badro, J., F. Ryerson, P.K. Weber, A. Ricolleau, S.J. Fallon, I.D. Hutcheon, F. Albarède, 2007, Chemical imaging with NanoSIMS: A window into deep-Earth geochemical processes. *Earth and Planetary Science Letters* 262, 543-551.

Bibak, A. and O.K. Borggaard, 1994, Molybdenum adsorption by aluminum and iron oxides and humic acid. *Soil Sci*., 158, 323-328.

Bradley, J.P., Z.R. Dai, R. Erni, N.D. Browning, G.A. Graham, P.K. Weber, J.B. Smith, I.D. Hutcheon, H. Ishii, S. Bajt, C. Floss, F.J. Stadermann, S. Sandford, 2005, An astronomical 2175 Å feature in interplanetary dust particles. *Science* 307, 244-247.

Chang, K.L.B., M. Tai, F. Cheng, 2001, Kinetics and products of the degradation of chitosan by hydrogen peroxide. *J. Agric. Food Chem.*, 49*,* 4845-4851.

Chang, J., Z. Kong, D. Hwang, K.L.B. Chang, 2006, Chitosan-catalyzed aggregation during the biomimetic synthesis of silica nanoparticles. *Chem. Mater.*, 18*,* 702-707.

Coradin, T. and J. Livage, 2001, Effect of some amino acids and peptides on silic acid polymerization. *Colloid. Surf. B: Biointerf.*, 21, 329-336

Coradin, T., O. Durupthy, J. Livage, 2002, Interactions of amino-containing peptides with sodium silicate and colloidal silica: a biomimetic approach of silicification. *Langmuir*, 18*,* 2331-2336.

Currie, H.A. and C.C. Perry, 2007, Silica in plants: biological, biochemical and chemical studies *Ann. Botany*, 100, 1383–1389.

Demadis, K.D. and E. Neofotistou, 2007, Synergistic effects of combinations of cationic polyaminoamide dendrimers/anionic polyelectrolytes on amorphous silica formation: a bioinspired approach. *Chem. Mater.*, 19*,* 581-587.

Ghosal, S., S.J. Fallon, T. Leighton, K.E. Wheeler, I.D. Hutcheon, P.K. Weber, 2008, Imaging and 3D elemental characterization of intact bacterial spores with high-resolution secondary ion mass spectrometry (NanoSIMS) depth profile analysis. *Analytical Chemistry*

Hallegot, P., R. Peteranderl, C. Lechene, 2004, In-situ imaging mass spectrometry analysis of melanin granules in the human hair shaft, *J. Invest. Derm.*, 122, 381-386.

Henriques, A.O. and C.P. Moran, 2000, Structure and assembly of the bacterial endospore coat. *Methods*, 20, 95-110.

Herrmann, A.M., P.L. Clode, I.R. Fletcher, N. Nunan, E.A. Stockdale, A.G. O'Donnell, D.V. Murphy, 2007, A novel method for the study of the biophysical interface in soils using nano-scale secondary ion mass spectrometry. *Rapid Commun. Mass Spectrom*. 21, 29–34

Kleinfeld, A.M., J.P. Kampf, C. Lechene, 2004 Transport of $^{13}$C-oleate in adipocytes measured using multi imaging mass spectrometry. *J. Am. Soc. Mass. Spectrom.*, 15, 1572–1580.

Kraft, M.L., P.K. Weber, M.L. Longo, I.D. Hutcheon, S.G. Boxer, 2006, Phase separation of lipid membranes analyzed with high-resolution secondary ion mass spectrometry. *Science*, 313, 1948-1951.

Kröger,N., R. Deutzmann, M. Sumper, 1999, Polycationic peptides from diatom biosilica that direct silica nanosphere formation. *Science* 286, 1129-1132.

Lechene, C. et. al., 2006, High-resolution quantitative imaging of mammalian and bacterial cells using stable isotope mass spectrometry. *J. Biol*., 20.1-20.30.

Leenheer, J.A., T.I. Noyes, C.E. Rostad, and M.L. Davisson, 2004, Characterization and origin of polar dissolved organic matter from the Great Salt Lake. *Biogeochemistry*. 69, 125-141.

McKeegan,K.D., et. al., 2006, Isotopic Compositions of cometary matter returned by Stardust. *Science*, 314, 1724-1728.

Moreau, J.W., P.K. Weber, M.C. Martin, B. Gilbert, I.D. Hutcheon, J.F. Banfield, 2007, Extracellular proteins limit the dispersal of biogenic nanoparticles. *Science* 316, 1600-1603.

Oehler, D.Z., F. Robert, S. Mostefaoui, A. Meibom, M. Selo, D.S. McKay, 2006, Chemical mapping of Proterozoic organic matter at submicron spatial resolution *Astrobiol*. 6, 838-850.

Phinney, D., 2006, Quantitative analysis of microstructures by secondary ion mass spectrometry. *Microsc. Microanal*., 12, 352-355.

Popa, R., P.K. Weber, J. Pett-Ridge, J.A. Finzi, S.J. Fallon, I.D. Hutcheon, K.H. Nealson, D.G. Capone, 2007, Carbon and nitrogen fixation and metabolite exchange in and between individual cells of *Anabaena oscillarioides*. *The International Society of Microbial Ecology Journal* 1, 354-360.

Seltmann, G. and O. Holst, 2002, *The Bacterial Cell Wall*. Springer-Verlag: Berlin

Standard Methods, 2005, *Standard Methods for the Examination of Water and Wastewater*. Joint publication of the American Public Health Association, the American Water Works Association, and the Water Environment Federation: Denver, CO.

Stevenson, F.J., 1994, *Humus Chemistry: Genesis, Composition, Reactions*. John Wiley and Sons, Inc.: New York, 496 pp.

Thurman, E.M. 1985. *Organic Geochemistry of Natural Waters*. Boston: Martinus Nijhoff/Dr W. Junk Publishers.

Wilson, R.G., F.A. Stevie, C.W. Magee, 1989, Secondary Ion Mass Spectrometry. John Wiley & Sons: New York, 384 pp.

## APPENDIX 1. Additional Materials Investigated for Use as Standards

### KBr+C+$SiO_2$ Pellets

Taking lessons from quantitative approaches used in spectroscopy, initial attempts used optical quality potassium bromide (KBr) as a matrix in which to incorporate various amounts of activated charcoal and silica. The contents of these mixtures were ground and blended in an agate mortar and pestle using a method typical for Fourier transform infrared spectroscopy KBr pellet preparation. The assumption using this approach is that blending would create particle sizes to at least that needed for FTIR analysis, or ≤1.0um scale. Mixtures were pressed in a standard 13 mm FTIR die cell for ~10 minutes at 13,000 pounds per square inch in order to form a KBr glass with a smooth surface. The samples were gold coated and then were placed in a standard NanoSims holder and measured using same tuning parameters used for Si analysis of biological spores. Unfortunately, initial attempts to measure the KBr suggested that electron charging was influencing the ionization efficiency of the sample. Furthermore, secondary ion images indicated that the substrate was not homogeneous and comprised various particle sizes. This approach was abandoned for the time being in order to pursue more promising materials.

### C-18 Solid Phase Extraction Media

C-18 solid phase extraction (SPE) media is a silica gel that is joined by siloxane bonds to hydrocarbons having 18 carbon backbones. The material is commonly used for the extraction of hydrophobic organic materials from solution. A 3 um mean diameter SPE was used for these exploratory measurements. The C-18 SPE particles were suspended in a few milliliters of distilled water and pipetted onto a silicon wafer and dried. The wafer was loaded into a standard NanoSims holder and gold coated. Samples were initial rastered with the $Cs^+$ for several minutes at high ionization current to facilitate element ionization. Apertures were adjusted to obtain ~6000 counts per second (cps) Si. Figures A-1a-d show the first five planes of images collected on a single particle. Note the carbon rim around the particle in Figure A-1a, which is consistent with the C-18 carbon chain bonded to the silica gel particle. The intensity of the carbon varied with depth and shifted position as the particle became smaller. Note that the absence Si counts in the central portion of the particle (Fig. A-1d) contrasts the Si-wafer on which it is mounted. This indicates the silica gel is charging and not readily yielding ions.

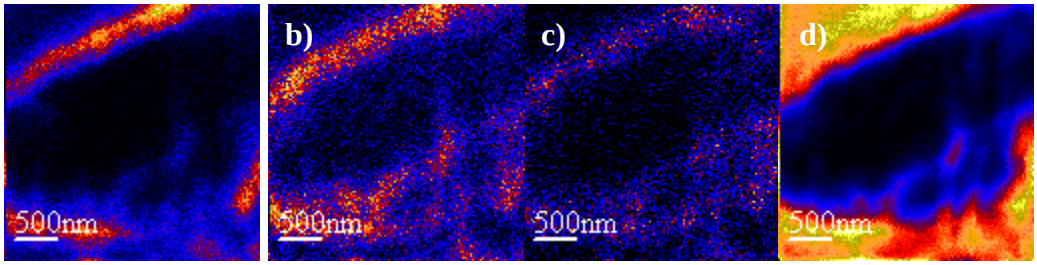


carbon chlorine fluorine silicon

**Figure A-1a-d -** Element images collected for C-18 SPE. Note a) the carbon-rich rim of the silica gel particle consistent with the C-18m molecules, with b) and c) minor levels of Cl and F, but d) the absence of Si in yielded from the silica particle.

The silica gel does not readily yield Si ions in the analysis, and carbon was found to be heterogeneously distributed in the ion images as the sample is rastered with depth. This causes an abnormal Si/C ratio and additional work trying to isolate regions of interest in the images for quantification. Therefore, the C-18 SPE was abandoned as a potential standard material for Si in biological materials.

### Polyglycol Lactic Acid Resin

These resins are water soluble materials that readily form spheroidal particles when ultrasonicated and dried. They were prepared separately for an unrelated research project whose goal was to develop standards for bioparticle detection. These samples were prepared free of Si and sized between 1um and 5um in diameter. Samples were mounted on an aluminum SEM stub, which was paced into a NanoSims holder. Below in Figure A-2 are 2um raster images of carbon from four sequential planes illustrated to show the variation in carbon with depth. This variation is characterized by a rapid decrease in carbon yield in the center of the sphere, suggesting that they may be hollow and carbon is predominantly observed on the edges. An ion count plot with depth in the 2um area is shown in Figure A-3 and illustrates the steady decrease in ion yield with depth.

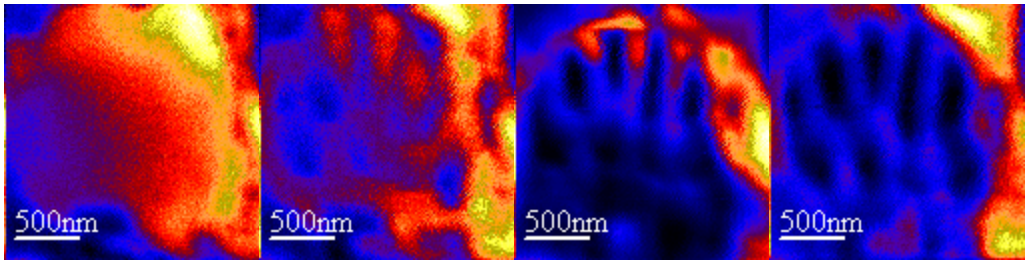


**Figure A-2** – Carbon ion images with depth from left to right illustrate the rapid decrease in carbon yield in the center of the sphere, consistent with being hollow.

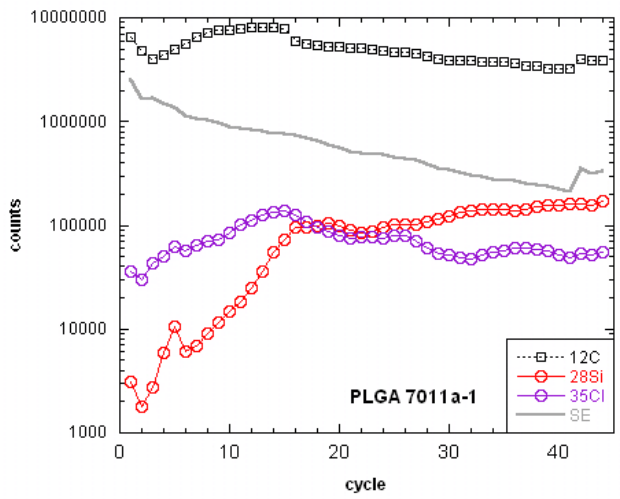


**Figure A-3**. Element concentrations with depth over one PLGA sphere. Note large variability in Si and carbon signals.

## Silicon Tubing

Silicon tubing comprises a polysiloxane polymer that is inert, heat resistant, and rubber-like. This material was explored as a possible standard with uniform Si content (in the percent range) in an organic matrix. A small piece of 5 mm i.d. tubing was used to obtain a thin slice of polymer that was subsequently gold-coated. This slice was not of uniform thickness, and was placed in a NanoSims holder and held in place with a stainless steel aperture. It was difficult to maintain flatness of the sample because of its flexibility and tendency to warp due to pressure from the aperture. Nevertheless, an attempt was made to analyze the sample. However, after several minutes of burn in time, the Si counts were still erratic and low. A second attempt was made to create a thinner and flatter sample by using the microtome device. After several attempts, the silicone tubing was abandoned because the rubber-like character of the material prevented a straight cut and always resulted in an uneven surface.

## APPENDIX 2 - Preparation Methods for Organic Colloids and Organic Fractions from Water and Air

Samples of aerosols/particulate matter and water will undergo a comprehensive chemical fractionation approach that isolates organic chemical classes based on size, water solubility, hydrophobicity, and ion-exchangeability. In the past eight years the mastery of a routine comprehensive fractionation and isolation scheme with 100% recovery has been obtained for aquatic humic substances (Leenheer et al., 2004). One of the key advancements is the recognition that colloidal size organics comprised a significant fraction of the dissolved organic matter, and these colloids were being irreversibly trapped onto the adsorptive resins. To overcome this, a dialysis step was introduced prior to resin adsorption. For water samples, this achieved a relatively pure isolation of a class of compounds resembling degraded bacterial cell walls. Lake sediment and peat soil extracts yield a nearly identical colloidal fraction. The permeate from the dialysis bags comprise lower molecular weight soluble compounds exhibiting hydrophobic, hydrophilic, and ionic character, and can be chemically fractionated in series with an ion exchange, XAD-8, and XAD-4 resins, followed by a detailed demineralization to isolate non-adsorbing organic compounds. The advantage of this reproducible and comprehensive isolation procedure is that all organic chemical classes represented in a given sample can 1) provide a unique fingerprint of their origin, 2) molecular structure and functional character without inorganic interferences, and 3) each class can be subsequently investigated further for isotopic abundances, presence of trace compounds, and molecular weight.

Organic aerosols collected on quartz filters, the comprehensive fractionation can be achieved by cutting up an appropriate amount of quartz filter (e.g. 20 mg as carbon) and placing into a dialysis bag with a 3500 Dalton (D) molecular weight permeate size. Waters can be rotoevaporated to a concentrate and placed in dialysis. Dialysis against a 0.1N HCl for 24 hours initially will ensure the dissolution of any carbonate minerals, which would later form insoluble minerals in dilute hydrofluoric acid. Likewise, many of the water-soluble organic compounds will be released from the bag at this time, and those with lower molecular weight will permeate through the bag. Dialysis with 0.2N HF follows in order to digest any silica. The HF step does not compromise the organic molecular character of the sample when digestion is completed at room temperature. Following the HF, the remaining material in the dialysis bag is dialyzed against 0.1N NaOH under $N_2$ to solubilize $AlF_3$, followed by distilled water until the conductivity of the permeate reaches <10 uS. This ensures the complete demineralization of the >3500 D organic isolate, or “colloid” fraction. The dialysis bag contents are then freeze-dried.

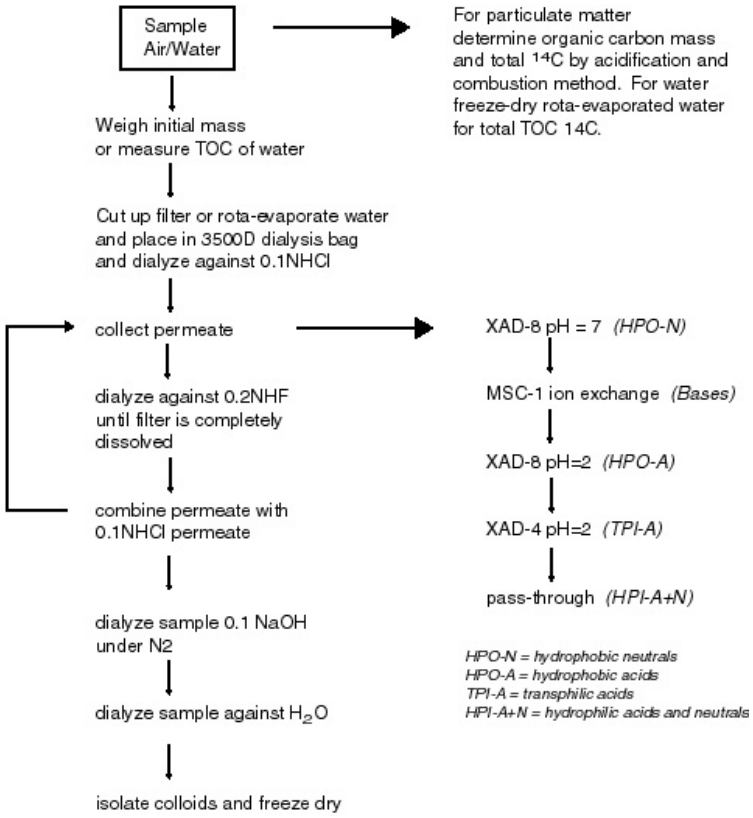


Dialysis bag permeates are collected as a single sample over the course of digestion. Typical collection volumes are around four liters. At this stage this entire volume is passed through a series of three resin columns. Firstly, permeate is brought to neutral pH and then passed through an XAD-8 column (at least 400 ml bed volume). The XAD-8 column is eluted with one bed volume of a 75% acetonitrile/25% $H_2O$ solvent, followed by a two bed volume rinse with distilled water. The eluate is then rota-evaporated to reduce volume and to remove acetonitrile. The remaining solution is freeze-dried to form a hydrophobic neutral (HPO-N) isolate. Pass-through solution is collected and adjusted to pH 2. Next, a MSC-1 cation exchange resin in the hydrogen form is connected in series to the XAD-8 followed by and XAD-4 resin column. Permeate (now at pH 2) is passed in series through the ion exchange, XAD-8, and XAD-4 columns. The pass-trough solution is collected. Each column is then eluted separately, the ion exchange eluted with 3N ammonium hydroxide, and the XAD-8 and XAD-4 eluted separately with a 75% acetonitrile/25% $H_2O$ solvent. Eluates are rota-evaporated and freeze-dried to form base, hydrophobic acid (HPO-A), and transphilic acid (TPI-A) isolates. The remaining permeate at this point undergoes a multi-step demineralization process, comprising pre-concentration, co-precipitation with glacial acidic acid, sulfate and phosphate removal by cationic salt formation, and nitrate and boron removal as volatile acids. Total mass of each isolate is measured either as total organic carbon in an aqueous solution using a Shimadzu 5000A TOC Analyzer, or measured gravimetrically as a solid.

## APPENDIX 3 – Preparation Method for Soil Humic Acid

Approximately one kilogram of soil was collected from a residential yard in Livermore, CA. The soil lay beneath irrigated lawn. The same was separated of its vegetative matter, including large roots. The remainder was freeze-dried. The freeze-dried material was crushed and sieved with a coarse screen. Small roots were removed as much as possible on the pass-through material. This material was then suspended and stirred overnight in a 0.1N NaOH solution. The next day the suspended solution was filtered at 1.0 um, and the filtrate was acidified to pH<2. The humic acid was allowed to precipitate and settle, followed by centrifugation to isolate. The isolated humic acid as then placed in a 3500 Dalton dialysis bag and dialyzed against 0.1HF overnight to remove as much silica as possible. The humic acid was then dialyzed against distilled water until a minimum conductivity was reached. This was followed by freeze-drying of the humic acid isolate for future use.